



CHORUS

This is the accepted manuscript made available via CHORUS. The article has been published as:

750 GeV diphoton excess explained by a resonant sneutrino in R-parity violating supersymmetry

B. C. Allanach, P. S. Bhupal Dev, S. A. Renner, and Kazuki Sakurai

Phys. Rev. D **93**, 115022 — Published 16 June 2016

DOI: [10.1103/PhysRevD.93.115022](https://doi.org/10.1103/PhysRevD.93.115022)

750 GeV Di-photon Excess Explained by a Resonant Sneutrino in R -parity Violating Supersymmetry

B. C. Allanach¹, P. S. Bhupal Dev^{2,3}, S. A. Renner¹, and Kazuki Sakurai⁴

¹*Department of Applied Mathematics and Theoretical Physics, Centre for Mathematical Sciences, University of Cambridge, Wilberforce Road, Cambridge CB3 0WA, UK*

²*Physik Department T30d, Technische Universität München, James-Frank-Straße 1, D-85748 Garching, Germany*

³*Max-Planck-Institut für Kernphysik, Saupfercheckweg 1, D-69117 Heidelberg, Germany and*

⁴*Institute for Particle Physics Phenomenology, Department of Physics, University of Durham, South Road, Durham DH1 3LE, UK*

We explain the recent excess seen by ATLAS and CMS experiments at around 750 GeV in the di-photon invariant mass as a narrow width sneutrino decaying to di-photons via a stau loop in R -parity violating Supersymmetry. The stau mass is predicted to be somewhere between half the resonant sneutrino mass and half the sneutrino mass plus 14 GeV. The scenario also predicts further signal channels at an invariant mass of 750 GeV, the most promising being into di-jets and WW . We also predict a left handed charged slepton decaying into WZ and $W\gamma$ at a mass 750-754 GeV.

I. INTRODUCTION

The ATLAS and CMS collaborations have recently presented the results of di-photon resonance searches in early Run II of $\sqrt{s} = 13$ TeV data [1–4]. For a spin-0 hypothesis, ATLAS observed an excess of 3.9σ local significance (2.0σ global) at a di-photon invariant mass of around 750 GeV with 3.2 fb^{-1} integrated luminosity. CMS also observed a 2.9σ excess locally (1.2σ globally) at a similar mass of 760 GeV in 3.3 fb^{-1} of data. The ATLAS excess prefers a large width ~ 45 GeV, but only at a very mild level (the local significance increases by 0.3σ above the narrow width approximation [3]), whereas the CMS fit prefers a much narrower width [4]. Together, these excesses are consistent with a new narrow-width resonance decaying into two photons with a cross-section of $\sigma(pp \rightarrow \gamma\gamma) \approx 5.3 \pm 2.4 \text{ fb}$ (unfolding efficiency and acceptance as in Ref. [5]¹). The possibility of a new 750 GeV resonance decaying into di-photons has stimulated a lot of interesting ideas and speculations in the theory community recently; for an incomplete list, see Refs. [5–91]. Many of the interpretations rely on heavy Higgs or other scalar bosons with additional charged particles that enhance the di-photon branching ratio and the total width.

In this work we interpret the observed di-photon excess *within* the Minimal Supersymmetric Standard Model (MSSM) framework as a 750 GeV scalar neutrino (sneutrino) resonance, $d\bar{d} \rightarrow \tilde{\nu}_i$, produced via the R -parity violating (RPV) interaction

$$W_{LV} = \lambda'_{i11} L_i Q_1 \bar{D}_1, \quad (1)$$

where i is the family index of the sneutrino. The sneutrino may decay into two photons through a stau loop with a left-right stau mixing via the RPV soft supersymmetry (SUSY) breaking term

$$\mathcal{L}_{LV}^{\text{soft}} = A_{i33} \tilde{\ell}_i \tilde{\ell}_3 \tilde{\tau}_R^\dagger + (\text{H.c.}), \quad (2)$$

where the $SU(2)_L$ indices of $\tilde{\ell}_i$ and $\tilde{\ell}_3$ are anti-symmetrically contracted implicitly, which forbids i to be 3, so the 750 GeV sneutrino has to be of electron or muon type in our scenario. There are two kinds of stau loops, as shown in Fig. 1, that will contribute to the di-photon signal and may explain the excesses observed in the ATLAS and CMS data, as shown below. Assuming that the resonance is a heavy neutral Higgs boson of the MSSM, the production cross section prediction is too small [9] unless additional non-MSSM states are added.² Thus, our interpretation in terms of one of the *only* other viable neutral scalars in the MSSM, namely a sneutrino, should serve as a well-motivated and minimal solution.

The rest of the paper is organised as follows. In Sec. II we consider the decay of the sneutrino and discuss the constraints on our scenario. In Sec. III we show our results and discuss the value of the sneutrino width that one

¹ This assumes efficiency times acceptance of 0.65 for ATLAS and 0.48 for CMS. These numbers were calculated assuming gluon fusion production, which will not be our case. However, to the accuracy with which we work, the approximation should be sufficiently good.

² However, neutral Higgs bosons in the NMSSM could explain the di-photon excess [92–94]. Another interesting possibility in spontaneously broken SUSY models is the goldstino [19, 21, 31, 95–97].

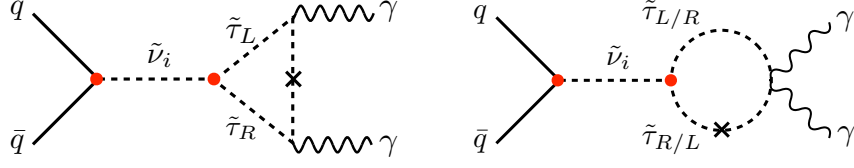


FIG. 1: Example Feynman diagrams for resonant sneutrino production via the $L_i Q_1 \bar{D}_1$ operator in Eq. (1) and its decay to two photons via the soft term $\tilde{\ell}_i \tilde{\ell}_3 \tilde{\tau}_R^+$ in Eq. (2). There are two kinds of diagrams: (*left*) through the triangle stau loop, and (*right*) through the $\tilde{\tau}_{R/L} \tilde{\tau}_{L/R}^* \gamma \gamma$ vertex, which must be included in the calculation to cancel the divergences in the loop integrals. The cross in the stau propagators represents the left-right mixing in the stau sector, which must be non-zero to have a di-photon signal.

can obtain in our scenario. In Sec. IV we show that all the relevant low-energy constraints can be satisfied for the di-photon favoured region in this model. Sec. V discusses how one might tweak the model in order to increase the width of the sneutrino in the event that it is unambiguously measured by the experiments to be a wide resonance. Sec. VI is devoted to conclusions.

II. SNEUTRINO DECAY

Given the interaction terms in Eq. (1), the sneutrino $\tilde{\nu}_i$ of mass $m_{\tilde{\nu}_i}$ may decay into $d\bar{d}$ with the following partial width:

$$\Gamma_{d\bar{d}} \equiv \Gamma(\tilde{\nu}_i \rightarrow d\bar{d}) = \frac{3}{16\pi} |\lambda'_{i11}|^2 m_{\tilde{\nu}_i}. \quad (3)$$

This decay is unavoidable because it is the inverse process to the production, and is constrained by the di-jet resonance searches [98, 99]. With the interaction terms in Eq. (2), the sneutrino may also decay into a pair of staus if $2m_{\tilde{\tau}_1} \leq m_{\tilde{\nu}_i}$, where $\tilde{\tau}_1$ is the lighter mass-eigenstate of the staus, with partial width

$$\Gamma_{\tilde{\tau}\tilde{\tau}} \equiv \Gamma(\tilde{\nu}_i \rightarrow \tilde{\tau}_1^+ \tilde{\tau}_1^-) = \frac{|A_{i33}|^2}{16\pi m_{\tilde{\nu}_i}} \left(1 - \frac{4m_{\tilde{\tau}_1}^2}{m_{\tilde{\nu}_i}^2}\right)^{1/2}, \quad (4)$$

where $m_{\tilde{\tau}_1}$ is the mass of the lightest stau. In this case, the branching ratio to the loop-induced di-photon decay mode shown in Fig. 1 will be hugely suppressed, thus disfavouring the di-photon signal. However, if the decay to on-shell staus is kinematically impossible ($2m_{\tilde{\tau}_1} > m_{\tilde{\nu}_i}$) and the hadronic decay in Eq. (3) is suppressed ($|\lambda'_{i11}| \ll 1$), the sneutrino can decay with an appreciable branching ratio into neutral gauge bosons $\gamma\gamma, \gamma Z, ZZ$ via the one-loop diagram of the staus shown in Fig. 1. Neglecting the contribution from the heavier state $\tilde{\tau}_2$, the partial widths are given by

$$\Gamma_{\gamma\gamma} \equiv \Gamma(\tilde{\nu}_i \rightarrow \gamma\gamma) = \frac{\alpha^2 m_{\tilde{\nu}_i}^3}{256\pi^3} \frac{|\bar{A}_{i33}|^2}{m_{\tilde{\tau}_1}^4} |A_0(\tau_{\tilde{\tau}})|^2, \quad (5)$$

$$\Gamma_{\gamma Z} \equiv \Gamma(\tilde{\nu}_i \rightarrow \gamma Z) = \frac{\alpha^2 m_{\tilde{\nu}_i}^3}{128\pi^3} \frac{|\bar{A}_{i33}|^2}{m_{\tilde{\tau}_1}^4} \left(1 - \frac{m_Z^2}{m_{\tilde{\nu}_i}^2}\right)^3 |\lambda_{Z\tilde{\tau}_1\tilde{\tau}_1} A_{0Z}(\tau_{\tilde{\tau}}^{-1}, \tau_Z^{-1})|^2, \quad (6)$$

$$\Gamma_{ZZ} \equiv \Gamma(\tilde{\nu}_i \rightarrow ZZ) = \frac{\alpha^2 m_{\tilde{\nu}_i}^3}{256\pi^3} \frac{|\bar{A}_{i33}|^2}{m_{\tilde{\tau}_1}^4} \left(1 - \frac{4m_Z^2}{m_{\tilde{\nu}_i}^2}\right)^3 |\lambda_{Z\tilde{\tau}_1\tilde{\tau}_1}^2 A_{0Z}(\tau_{\tilde{\tau}}^{-1}, \tau_Z^{-1})|^2, \quad (7)$$

where $\bar{A}_{i33} \equiv A_{i33} \cos\theta \sin\theta$, $\lambda_{Z\tilde{\tau}_1\tilde{\tau}_1} \equiv a - b \cos 2\theta$, with $a \equiv (3 \tan\theta_w - \cot\theta_w)/4$, $b \equiv (\tan\theta_w + \cot\theta_w)/4$, θ_w being the weak mixing angle and θ being the left-right mixing angle of the stau sector: i.e. $\tilde{\tau}_{R/L} = \tilde{\tau}_{1/2} \cos\theta \pm \tilde{\tau}_{2/1} \sin\theta$. Also, $\tau_{\tilde{\tau}} \equiv m_{\tilde{\nu}_i}^2/4m_{\tilde{\tau}_1}^2$, $\tau_Z \equiv m_Z^2/4m_{\tilde{\tau}_1}^2$ and the scalar loop functions A_0 and A_{0Z} are defined by

$$A_0(x) = -\frac{x - f(x)}{x^2}, \quad (8)$$

$$A_{0Z}(x_1, x_2) = \frac{x_1 x_2}{2(x_1 - x_2)} + \frac{x_1^2 x_2^2}{2(x_1 - x_2)^2} [f(x_1^{-1}) - f(x_2^{-1})] \\ + \frac{x_1^2 x_2}{(x_1 - x_2)^2} [g(x_1^{-1}) - g(x_2^{-1})], \quad (9)$$

where the functions f and g are

$$f(x) = \begin{cases} \arcsin^2(\sqrt{x}) & \text{if } x \leq 1 \\ -\frac{1}{4} \left[\log \left(\frac{1+\sqrt{1-1/x}}{1-\sqrt{1-1/x}} \right) - i\pi \right]^2 & \text{if } x > 1, \end{cases} \quad (10)$$

$$g(x) = \begin{cases} \frac{\sqrt{1-1/x}}{2} \left[\log \left(\frac{1+\sqrt{1-1/x}}{1-\sqrt{1-1/x}} \right) - i\pi \right] & \text{if } x < 1 \\ \sqrt{1/x-1} \arcsin(\sqrt{x}) & \text{if } x \geq 1. \end{cases} \quad (11)$$

One can see that these partial widths are proportional to $\sin 2\theta$ through \bar{A}_{i33} , meaning that a large left-right mixing is required to obtain a large di-photon branching ratio. This can also be understood diagrammatically due to the presence of the cross on the stau propagator in Fig. 1.³ If the stau sector has a large left-right mixing, one tends to have a large mass hierarchy, $m_{\tilde{\tau}_2} \gg m_{\tilde{\tau}_1}$. We can therefore neglect the $\tilde{\tau}_2$ contribution in the loop. On the other hand, the $\tilde{\nu}_\tau$ contribution relevant for the $\tilde{\nu}_i \rightarrow W^+W^-$ decay mode through the $\tilde{\tau}_L - \tilde{\tau}_R - \tilde{\nu}_\tau$ triangle loop need not be negligible in the large mixing limit. To be precise, the WW partial width in the limit $m_{\tilde{\tau}_2} \gg m_{\tilde{\tau}_1}$ is given by

$$\begin{aligned} \Gamma_{WW} \equiv \Gamma(\tilde{\nu}_i \rightarrow W^+W^-) &= \frac{\alpha_w^2 m_{\tilde{\nu}_i}^3 |\bar{A}_{i33}|^2}{1024\pi^3 m_{\tilde{\tau}_1}^4} \sin^4 \theta \left(1 - \frac{4m_W^2}{m_{\tilde{\nu}_i}^2} \right)^{1/2} \\ &\times \left[\frac{|F|^2}{16\tau_{\tilde{\tau}}^2} \left(12 - \frac{4m_{\tilde{\nu}_i}^2}{m_W^2} + \frac{m_{\tilde{\nu}_i}^4}{m_W^4} \right) - \frac{|F \cdot G|}{2\tau_{\tilde{\tau}}} \left(8 - \frac{6m_{\tilde{\nu}_i}^2}{m_W^2} + \frac{m_{\tilde{\nu}_i}^4}{m_W^4} \right) + |G|^2 \left(16 - \frac{8m_{\tilde{\nu}_i}^2}{m_W^2} + \frac{m_{\tilde{\nu}_i}^4}{m_W^4} \right) \right], \end{aligned} \quad (12)$$

where $\alpha_w \equiv g_w^2/4\pi$, g_w is the $SU(2)_L$ gauge coupling, and

$$F(m_{\tilde{\nu}_i}^2, m_{\tilde{\tau}_1}^2, m_{\tilde{\nu}_\tau}^2, m_W^2) = 2C_{00}(m_{\tilde{\nu}_i}^2, m_W^2, m_W^2, m_{\tilde{\tau}_1}^2, m_{\tilde{\tau}_1}^2, m_{\tilde{\nu}_\tau}^2) - \frac{1}{2}B_0(m_{\tilde{\nu}_i}^2, m_{\tilde{\tau}_1}^2, m_{\tilde{\tau}_1}^2), \quad (13)$$

$$\begin{aligned} G(m_{\tilde{\nu}_i}^2, m_{\tilde{\tau}_1}^2, m_{\tilde{\nu}_\tau}^2, m_W^2) &= m_{\tilde{\tau}_1}^2 [C_{11}(m_{\tilde{\nu}_i}^2, m_W^2, m_W^2, m_{\tilde{\tau}_1}^2, m_{\tilde{\tau}_1}^2, m_{\tilde{\nu}_\tau}^2) \\ &\quad + C_{12}(m_{\tilde{\nu}_i}^2, m_W^2, m_W^2, m_{\tilde{\tau}_1}^2, m_{\tilde{\tau}_1}^2, m_{\tilde{\nu}_\tau}^2) \\ &\quad + C_1(m_{\tilde{\nu}_i}^2, m_W^2, m_W^2, m_{\tilde{\tau}_1}^2, m_{\tilde{\tau}_1}^2, m_{\tilde{\nu}_\tau}^2)] \end{aligned} \quad (14)$$

with $B_0, C_1, C_{00,11,12}$ being the usual scalar two- and three-point Passarino-Veltman functions [100] in the conventions of Ref. [101], which we evaluate numerically using `LoopTools` [102]. From Eqs. (5) and (12), we find that the WW partial width can be suppressed with respect to the di-photon width by a suitable choice of the mass and mixing parameters in the stau sector.

The total decay width Γ_{tot} of the sneutrino in our scenario is thus given by

$$\Gamma_{\text{tot}} \simeq \Gamma_{d\bar{d}} + \Gamma_{\tilde{\tau}\tilde{\tau}} + \Gamma_{\gamma\gamma} + \Gamma_{\gamma Z} + \Gamma_{ZZ} + \Gamma_{WW} + \Gamma_X, \quad (15)$$

where the partial widths are given in Eqs. (3)-(7) and (12), and Γ_X is the contribution from any other possible decay channels not explicitly mentioned here but that could potentially have an appreciable partial width (by changing model parameters and making other super partners non-decoupled).

For a numerical illustration, we choose the following benchmark values for the stau sector:

$$\begin{aligned} \tilde{m}_{L_3}^2 &= m_{\tilde{e}_3}^2 + m_\tau^2 + m_Z^2 \cos 2\beta \left(-\frac{1}{2} + \sin^2 \theta_w \right) = (425 \text{ GeV})^2, \\ \tilde{m}_{R_3}^2 &= m_{\tilde{\tau}_R}^2 + m_\tau^2 - m_Z^2 \cos 2\beta \sin^2 \theta_w = (445 \text{ GeV})^2, \\ X_\tau &= m_\tau(A_\tau - \mu \tan \beta) = -43 \text{ GeV}^2, \\ \tan \beta &= 20. \end{aligned} \quad (16)$$

The stau mass-squared matrix in the gauge eigenbasis $(\tilde{\tau}_L, \tilde{\tau}_R)$ is given by

$$M_{\tilde{\tau}}^2 = \begin{pmatrix} \tilde{m}_{L_3}^2 & X_\tau \\ X_\tau & \tilde{m}_{R_3}^2 \end{pmatrix}, \quad (17)$$

³ In principle, one can also allow for a large mixing in the selectron or smuon sector with a large μ -term and/or large $\tan \beta$, albeit with some tuning of the parameters to avoid tachyonic states. Our subsequent analysis is equally applicable to these cases, but we stick to staus for definiteness.

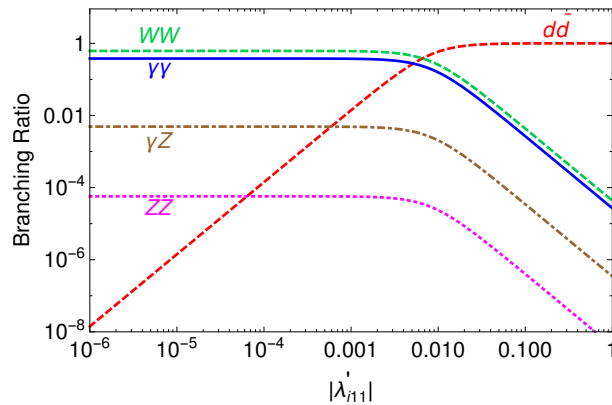


FIG. 2: The branching ratios of the sneutrino decay to $d\bar{d}$, $\gamma\gamma$, γZ , ZZ and WW . Here we have chosen the benchmark values given in Eq. (18), in addition to setting $m_{\tilde{\nu}_i} = 750$ GeV and $A_{i33} = 14 m_{\tilde{\tau}_1}$.

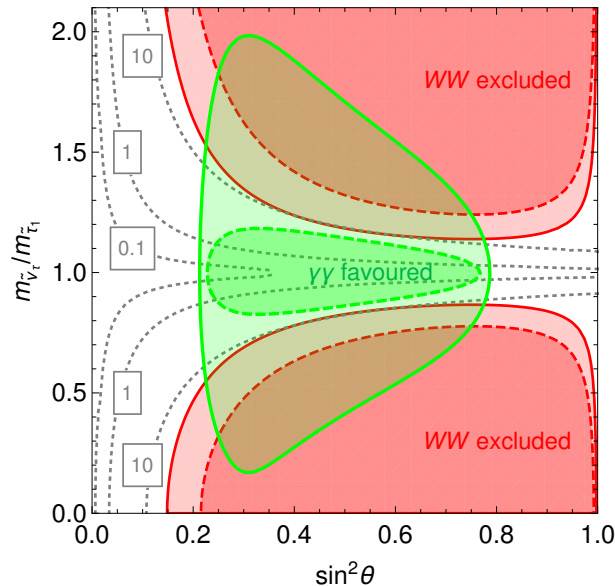


FIG. 3: The contours of $BR_{WW}/BR_{\gamma\gamma}$ (dotted curves) as a function of the stau mixing angle θ and the mass ratio $m_{\tilde{\nu}_\tau}/m_{\tilde{\tau}_1}$ for fixed values of $m_{\tilde{\tau}_1} = 380$ GeV, $m_{\tilde{\nu}_i} = 750$ GeV and $A_{i33} = 14 m_{\tilde{\tau}_1}$. The red-shaded regions enclosed by the red solid (dashed) curves are the 95% CL exclusion regions for $|\lambda'_{i11}| = 0.08$ (0.02) from the $\sqrt{s} = 8$ TeV LHC WW data. The green-shaded regions enclosed by the green solid (dashed) curves are the 1σ favoured regions for $|\lambda'_{i11}| = 0.08$ (0.02) to explain the $\sqrt{s} = 13$ TeV LHC di-photon excess.

with the left-right stau mixing given by $\tan 2\theta = 2X_\tau/(\tilde{m}_{L_3}^2 - \tilde{m}_{R_3}^2)$. The tau sneutrino mass is given by $m_{\tilde{\nu}_\tau}^2 = m_{\tilde{\ell}_3}^2 + (1/2)m_Z^2 \cos 2\beta$. Thus, Eqs. (16) lead to the following mass and mixing values:

$$m_{\tilde{\tau}_1} = 382 \text{ GeV}, \quad m_{\tilde{\tau}_2} = 483 \text{ GeV}, \quad m_{\tilde{\nu}_\tau} = 416 \text{ GeV}, \quad \sin^2 \theta = 0.4. \quad (18)$$

We now compute the branching ratios of the sneutrino decay to di-jet, di-photon, γZ , ZZ and WW channels using Eq. (18). This is shown in Fig. 2 for a suitable choice of parameters $m_{\tilde{\nu}_i} = 750$ GeV and $A_{i33} = 14 m_{\tilde{\tau}_1}$. From Fig. 2, we find that the di-photon branching ratio is sizable for small λ'_{i11} , which however cannot be made arbitrarily small, since the sneutrino production cross section is proportional to $|\lambda'_{i11}|^2$. We also note that the partial widths for $\tilde{\nu}_i \rightarrow \gamma Z$ and $\tilde{\nu}_i \rightarrow ZZ$ are respectively $\sim 10^{-2}$ and $\sim 10^{-4}$ of $\Gamma_{\gamma\gamma}$.

On the other hand, the WW partial width can be comparable to or larger than the di-photon width, depending on the stau mixing and tau sneutrino mass, as depicted in Fig. 3. In particular, for smaller stau mixing, the WW rate is suppressed with respect to the $\gamma\gamma$ due to the additional $\sin^4 \theta$ dependence in Eq. (12), but we cannot take the mixing to be arbitrarily small, as it would also suppress the $\gamma\gamma$ rate with respect to the di-jet rate. We find that θ must be between $\pi/7$ and $\pi/3$ to have a di-photon favoured region consistent with other constraints (see Section III). Similarly,

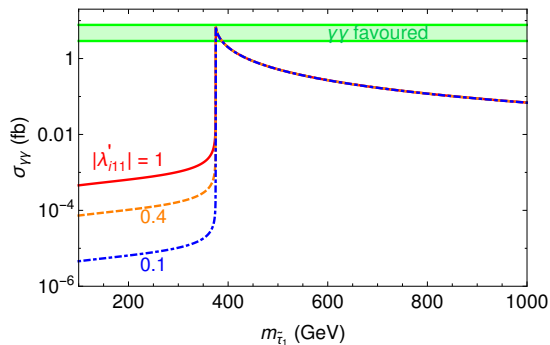


FIG. 4: The di-photon signal cross section times branching ratio as a function of the stau mass for different values of the RPV coupling λ'_{i11} .

if the tau sneutrino mass is close to the stau mass, the ratio $\text{BR}_{WW}/\text{BR}_{\gamma\gamma}$ is small, giving a larger parameter space for the di-photon signal. In Fig. 3, the red-shaded regions enclosed by the red solid (dashed) curves are the 95% CL exclusion regions for $|\lambda'_{i11}| = 0.08$ (0.02) from the $\sqrt{s} = 8$ TeV LHC WW data [103, 104]. The green-shaded regions enclosed by the green solid (dashed) curves are the 1σ favoured regions for $|\lambda'_{i11}| = 0.08$ (0.02) to explain the $\sqrt{s} = 13$ TeV LHC di-photon excess [3, 4]. Here, we cannot take a larger value of $|\lambda'_{i11}|$, otherwise it will be in conflict with the $\sqrt{s} = 8$ TeV di-jet constraints [98, 99] (see Fig. 5). A smaller value of $|\lambda'_{i11}|$ will give a smaller di-photon favoured region. We see from the figure that there is ample room in parameter space where a resonant sneutrino fits the di-photon excess whilst simultaneously satisfying constraints on resonant WW production.

III. RESULTS

We compute the signal cross section at $\sqrt{s} = 13$ TeV LHC using the RPV model implementation in `FeynRules` [105] and the parton-level event generation in `MadGraph5` [106] with `NNPDF2.3` leading order parton distribution functions [107]. We find

$$\sigma(pp \rightarrow \tilde{\nu}_i \rightarrow \gamma\gamma)_{13\text{TeV}} = \sigma_0^{13\text{TeV}} |\lambda'_{i11}|^2 \cdot \text{BR}_{\gamma\gamma}, \quad (19)$$

where $\sigma_0^{13\text{TeV}} = 156$ pb for $m_{\tilde{\nu}_i} = 750$ GeV with $\lambda'_{i11} = 1$. We require that the signal cross section be within the 1σ region of the observed value, i.e. 5.3 ± 2.4 fb [5]. Fig. 4 shows predictions for the signal cross section times branching ratio as a function of the lightest stau mass for different values of λ'_{i11} . When the stau mass is smaller than half the resonant sneutrino mass at the left-hand side of the plot, the branching ratio to the di-photon channel is highly suppressed and consequently the signal cross section is much too small. It is clear from the figure that when the stau mass is half (or just over half) the resonant sneutrino mass, the cross section fits the di-photon excess measurements. Here, on-shell stau production is kinematically disfavoured, boosting the $\gamma\gamma$ branching ratio, but as the stau mass further increases, the loop diagram depicted in Fig. 1 becomes increasingly mass suppressed and the signal cross section dies off.

There exist constraints on the di-boson decay modes from the 8 TeV LHC data [14]. For the benchmark point shown in Figure 2a, all these constraints are satisfied, except that there is a small 2σ level tension in the $\gamma\gamma$ channel between the Run-I and Run-II data sets for the production mode through $d\bar{d}$ annihilation, as considered here.

On the other hand, the $\tilde{\nu}_i \rightarrow d\bar{d}$ channel is constrained by the di-jet resonance searches [98, 99]. The most stringent constraint comes from the $\sqrt{s} = 8$ TeV LHC data [108]⁴:

$$\sigma(pp \rightarrow \tilde{\nu}_i \rightarrow d\bar{d})_{8\text{TeV}} \simeq \sigma_0^{8\text{TeV}} |\lambda'_{i11}|^2 \cdot \text{BR}_{d\bar{d}} \lesssim 0.9 \text{ pb}, \quad (20)$$

where $\sigma_0^{8\text{TeV}} = 57$ pb is the $\sqrt{s} = 8$ TeV production cross section for $pp \rightarrow \tilde{\nu}_i$ with $\lambda'_{i11} = 1$ and $\text{BR}_{d\bar{d}} = \Gamma_{d\bar{d}}/\Gamma_{\text{tot}}$ is the branching ratio of the di-jet decay mode.

⁴ Note that the reported results from the early Run II LHC di-jet resonance searches [109, 110] do not cover the region at di-jet invariant masses of 750 GeV at all.

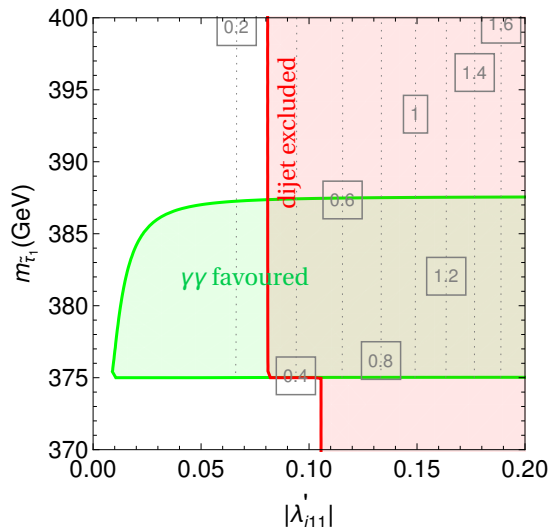


FIG. 5: The preferred region for the di-photon excess (green) and the excluded region from the di-jet resonance search (red), assuming there is no other decay channel than $d\bar{d}$, $\gamma\gamma$, γZ , ZZ and WW . The dashed contours show the total decay width of the sneutrino in GeV.

Let us first consider the $\Gamma_X = 0$ case. Since the upper limit of the di-jet cross section (0.9 pb) is much larger than the preferred di-photon cross section (8 fb), we have $\Gamma_{d\bar{d}} \gg \Gamma_{\gamma\gamma}$ in the most of the interesting parameter region. In this regime the total width of the sneutrino can be approximated by $\Gamma_{d\bar{d}} \approx |\lambda'_{i11}|^2$ and we have

$$\sigma(pp \rightarrow \tilde{\nu}_i \rightarrow \gamma\gamma) \approx |\lambda'_{i11}|^2 \cdot \left(\frac{\Gamma_{\gamma\gamma}}{|\lambda'_{i11}|^2} \right) \propto \Gamma_{\gamma\gamma}, \quad (21)$$

$$\sigma(pp \rightarrow \tilde{\nu}_i \rightarrow d\bar{d}) \approx |\lambda'_{i11}|^2 \cdot \left(\frac{\Gamma_{d\bar{d}}}{|\lambda'_{i11}|^2} \right) \propto |\lambda'_{i11}|^2. \quad (22)$$

Thus, the $\gamma\gamma$ signal rate is approximately independent of λ'_{i11} as Fig. 4 shows in the region $m_{\tilde{\tau}_1} > m_{\tilde{\nu}_i}/2$.

The di-jet signal cross section also receives a contribution from charged slepton production:

$$\sigma(pp \rightarrow \tilde{e}_{L_i}^- \rightarrow \bar{u}d) = \sigma_-^{8 \text{ TeV}} |\lambda'_{i11}|^2 \text{BR}(\tilde{e}_{L_i}^- \rightarrow \bar{u}d), \quad (23)$$

$$\sigma(pp \rightarrow \tilde{e}_{L_i}^+ \rightarrow u\bar{d}) = \sigma_+^{8 \text{ TeV}} |\lambda'_{i11}|^2 \text{BR}(\tilde{e}_{L_i}^+ \rightarrow u\bar{d}). \quad (24)$$

In the following discussion, we assume $\text{BR}(\tilde{e}_{L_i}^\pm \rightarrow u\bar{d}/\bar{u}d) = 1$ for simplicity. This leads to an conservative upper limit on $|\lambda'_{i11}|$ from the di-jet constraint, which could be somewhat relaxed for $\text{BR}(\tilde{e}_{L_i}^\pm \rightarrow u\bar{d}/\bar{u}d) < 1$. We also assume that the LR mixing in the \tilde{e}_i^\pm sector is negligible. This is justified since the LR mixing is proportional to the fermion mass, which is negligible for first two generations. At tree level, we have $m_{\tilde{e}_{L_i}}^2 = m_{\tilde{\nu}_i}^2 - M_W^2 \cos 2\beta$; thus in the range of $\beta \in [\pi/4, \pi/2]$ considered, $750 < m_{\tilde{e}_i}/\text{GeV} < 754$ for $m_{\tilde{\nu}_i} = 750$ GeV. This means that the sum of Eqs. (22), (23) and (24) is constrained by the di-jet bound: we have included each in the calculation of the bound in Fig. 5. We obtain $\sigma_-^{8 \text{ TeV}} = 23$ pb and $\sigma_+^{8 \text{ TeV}} = 57$ pb for a 750 GeV charged slepton. The charged slepton has decays into $W\gamma$ or WZ via a loop of stau/stau-sneutrino, with expected partial widths of the same order as the WW and $\gamma\gamma$ partial width of the sneutrino. These channels therefore bring additional verification possibilities.

Fig. 5 shows our numerical result for the $\Gamma_X = 0$ case. Throughout this section, we take the near-maximal left-right mixing with $\sin^2 \theta = 0.4$ and $A_{i33} = 14 m_{\tilde{\tau}_1}$ so that the signal rate is enhanced without too much fine-tuning.⁵ In the

⁵ The signal rate is maximized for $\theta = \pi/4$ and $m_{\tilde{\nu}_\tau} = m_{\tilde{\tau}_1}$ which is possible, but requires a large fine-tuning with $\tilde{m}_{L3}^2 = \tilde{m}_{R3}^2$ in Eq. (17). Also note that the chosen value of A_{i33} is roughly at the upper limit from perturbativity arguments [111]: larger values of A_{i33} generate a large $|\tilde{\ell}_i|^4$ operator via a one-loop box diagram involving a loop of $\tilde{\tau}_1$ [111]. There have been arguments proposed (see e.g. [112]) to the effect that such a large trilinear coupling may destabilise the potential at large field values of $\tilde{\tau}_1$. In this case, additional (non-MSSM) heavy states would be required to modify the high energy behaviour of the potential such that the stability of the vacuum is restored, even with the large value of A_{i33} chosen here. Another resolution of the stability would be to lower A_{i33} and

green shaded region, the di-photon signal rate is within the 1σ band of the observed value, whereas the red shaded region is excluded by the di-jet resonance searches. As discussed above, the signal rate depends almost exclusively on $m_{\tilde{\tau}_1}$ unless $|\lambda'_{i11}| \ll 1$. As can be seen, in order to explain the di-photon excess the lightest stau mass must be within the narrow window $375 \text{ GeV} \leq m_{\tilde{\tau}_1} \lesssim 389 \text{ GeV}$. The lower mass limit is required to forbid the two-body decay mode, $\tilde{\nu}_i \rightarrow \tilde{\tau}_1^+ \tilde{\tau}_1^-$. Above this kinematical threshold, one observes gradual suppression with stau mass due to gradual decoupling. For a smaller value of A_{i33} or θ , the upper limit on the stau mass becomes stronger and the green-shaded region in Fig. 5 shrinks, until we have no allowed region left for $A_{i33} < 10 m_{\tilde{\tau}_1}$ or for $\theta < \pi/7$. Contrary to the di-photon rate, the di-jet constraint is sensitive to $|\lambda'_{i11}|$ and excludes the region where $|\lambda'_{i11}| > 0.08$.

The dashed contours in Fig. 5 show the total decay width of the sneutrino in GeV. As we discussed previously, the total width is dominated by the $\tilde{\nu}_i \rightarrow d\bar{d}$ mode and depends only on $|\lambda'_{i11}|$ unless $|\lambda'_{i11}| \ll 1$. As can be seen, $\Gamma_{\text{tot}} > 300 \text{ MeV}$ is excluded by the di-jet constraint in the region favoured by the di-photon excess. This is a prediction of the model in its minimal version: *if the signal persists and the resonance is better resolved, it should have a narrow width.*

IV. LOW-ENERGY CONSTRAINTS

We must make sure that the di-photon favoured range of λ'_{i11} in Fig. 5 is consistent with other low-energy constraints, such as electroweak precision observables and lepton flavour violating processes [113].⁶ For instance, the constraint from charged current universality in lepton and quark sectors implies [116, 117]

$$\lambda'_{11k} \leq 0.02 \left(\frac{m_{\tilde{d}_{kR}}}{100 \text{ GeV}} \right). \quad (25)$$

Similar limits on λ'_{11k} are also obtained from atomic parity violation in ^{133}Cs [113]. From neutrino-lepton elastic scattering mediated by neutral currents, we get [113]

$$\lambda'_{21k} \leq 0.15 \left(\frac{m_{\tilde{d}_{kR}}}{100 \text{ GeV}} \right), \quad \lambda'_{2j1} \leq 0.18 \left(\frac{m_{\tilde{d}_{jL}}}{100 \text{ GeV}} \right). \quad (26)$$

Large λ'_{i11} interactions can also induce sizable lepton flavour violating radiative decays of charged leptons [118]. Using the most stringent constraint from MEG on $\text{BR}(\mu \rightarrow e\gamma) < 5.7 \times 10^{-13}$ at 90% C.L. [119], we obtain

$$|\lambda'_{2jk}\lambda'_{1jk}| \lesssim 1.6 \times 10^{-5} \left(\frac{m_{\tilde{d}_{kR}}}{100 \text{ GeV}} \right)^2. \quad (27)$$

Limits on $|\lambda'_{i11}|$ were also set from the electric dipole moment (EDM) constraints [120]. Using the current best upper limit on electron EDM, $|d_e| < 8.7 \times 10^{-29} e \cdot \text{cm}$ at 90% C.L. [121], we get $|\lambda'_{i11}| \leq 9.3 \times 10^{-6}$, whereas from muon EDM, we get a much weaker constraint: $|\lambda'_{211}| \leq 0.5$, assuming all the relevant squark and slepton masses in the loop to be 100 GeV. These limits can however be completely evaded by a suitable choice of phases in the squark mixing matrix or at least significantly weakened by making the squarks heavier: already if they are placed at 1 TeV, the above constraints leave plenty of room for the values of $\lambda'_{i11} < 0.1$ that we require to explain the di-photon resonance.

For $i = 1$, the λ'_{111} coupling is also constrained by neutrinoless double beta decay ($0\nu\beta\beta$) [122, 123]. Using the current 90% CL combined limit on the $0\nu\beta\beta$ half-life for ^{76}Ge isotope from GERDA phase-I: $T_{1/2}^{0\nu} > 3.0 \times 10^{25} \text{ yr}$ [124], we find [125, 126]

$$|\lambda'_{111}| \lesssim 4.5 \times 10^{-4} \left(\frac{m_{\tilde{e}_L}}{100 \text{ GeV}} \right)^2 \left(\frac{m_{\tilde{\chi}_1^0}}{100 \text{ GeV}} \right)^{1/2} \simeq 0.025 \left(\frac{m_{\tilde{\chi}_1^0}}{100 \text{ GeV}} \right)^{1/2} \quad (28)$$

enhance the signal rate by using additional sneutrino states in the loop. For instance, if $m_{\tilde{\nu}_e} \simeq m_{\tilde{\nu}_\mu} \simeq 750 \text{ GeV}$, one can obtain an enhancement factor of $2^2 = 4$, although in this case the mass splitting between the sneutrinos would need to be smaller than their $\mathcal{O}(1 \text{ GeV})$ widths. One could also have additional enhancement from a smuon contribution in the loop, where non-zero A_{i22} as well as a light $\tilde{\mu}_1$ with a large mixing between left and right handed smuons would be required. Yet another possibility is to produce $\tilde{\nu}_i$ from a cascade decay of $\tilde{e}_{L_i}^\pm$ as $pp \rightarrow \tilde{e}_{L_i}^\pm \rightarrow W^\pm \tilde{\nu}_i$. This requires large LR mixing in the light-flavour slepton sectors in order to have a large enough mass splitting between \tilde{e}_i^\pm and $\tilde{\nu}_i$ to allow this decay. Since the current di-photon excess has only ~ 20 events, having this sub-leading contribution with an extra W boson is still consistent with data. In this case, the di-jet constraint is also relaxed because $\text{BR}(\tilde{e}_{L_i}^\pm \rightarrow u\bar{d}/\bar{u}d) < 1$.

⁶ For detailed discussions of the indirect constraints on the scalar di-photon resonance, see Refs. [114, 115].

for a selectron mass of 750 GeV. Comparing this with the di-photon favoured region in Fig. 5, we find that the $0\nu\beta\beta$ constraint still allows some parameter space for the $i = 1$ case as long as the lightest neutralino is heavier than about 50 GeV. We also note that our scenario satisfies the constraints from S and T parameters measured at LEP, since the sleptons are heavier than 375 GeV. For details, see Fig. 3 of Ref. [127].

To summarize, the low-energy constraints depend on additional sparticle masses not involved in the di-photon explanation, and are easily satisfied by making the sparticles appropriately heavy enough, without affecting the di-photon signal.

V. MODEL TWEAKS

One way to increase Γ_{tot} would be to allow the sneutrino to have other decay modes, X . If Γ_X were as large as or larger than $\Gamma_{d\bar{d}}$, the cross sections would scale as

$$\begin{aligned}\sigma(pp \rightarrow \tilde{\nu}_i \rightarrow \gamma\gamma) &\propto |\lambda'_{i11}|^2 \left(\frac{\Gamma_{\gamma\gamma}}{c|\lambda'_{i11}|^2 + \Gamma_X} \right), \\ \sigma(pp \rightarrow \tilde{\nu}_i \rightarrow d\bar{d}) &\propto |\lambda'_{i11}|^2 \left(\frac{c|\lambda'_{i11}|^2 + \delta_{1n}\Gamma_X}{c|\lambda'_{i11}|^2 + \Gamma_X} \right), \\ \sigma(pp \rightarrow \tilde{\nu}_i \rightarrow X) &\propto |\lambda'_{i11}|^2 \left(\frac{\Gamma_X}{c|\lambda'_{i11}|^2 + \Gamma_X} \right),\end{aligned}\tag{29}$$

where c is some constant. A few remarks can be made. First of all, all processes depend on Γ_X . Second, the di-photon rate now also depends on λ'_{i11} . Therefore, for $\Gamma_X > 0$, to compensate for the suppression in the di-photon rate, a larger value of $|\lambda'_{i11}|$ will be preferred. The suffix n of the Kronecker delta is 0 except for $X = d_k\bar{d}_l$ with d_k being one of d, s, b (and \bar{d}_l being one of $\bar{d}, \bar{s}, \bar{b}$) excluding $X = d\bar{d}$. These decay modes can be opened up by introducing a non-zero λ'_{ikl} coupling for the $L_i Q_k \bar{D}_l$ operator in the superpotential in Eq. (1). For $n = 1$, the di-jet cross section is independent of Γ_X , whereas it is suppressed with $\Gamma_X > 0$ for the $n = 0$ case.

Appropriate constraints on $\sigma(pp \rightarrow \tilde{\nu}_i \rightarrow X)$ should be taken into account⁷. For example, if some of the neutralinos and charginos are lighter than $\tilde{\nu}_i$, one can consider $\tilde{\nu}_i \rightarrow \nu\tilde{\chi}_j^0$ and $\tilde{\nu}_i \rightarrow \ell^\pm\tilde{\chi}_j^\mp$. In RPV scenarios, the χ_j^0 and χ_j^\pm subsequently decay into jets and leptons via RPV interactions and these processes may be observed as multi-jet and/or multi-lepton with or without large missing transverse momentum final states. Constraints on these processes depend on the details of the final state particles and the masses of χ_j^0 and χ_j^\pm , but are typically more stringent than the di-jet constraint. Another possibility is $X = b\bar{b}$ or $b\bar{s}$ ($s\bar{b}$). The upper bound on the $b\bar{b}$ signal cross-section is about 1 pb from the di-bottom resonance search [129], whilst the latter does not have any other constraint apart from the di-jet constraint previously covered.

Additionally, one could tweak the model to explain a wider peak by having multiple sneutrino resonances, e.g. $\tilde{\nu}_e$ and $\tilde{\nu}_\mu$, with slightly different masses, $\Delta m \sim \mathcal{O}(10)$ GeV: at present, statistics are such that one cannot resolve these two different masses with the ATLAS data presented, however this tweak predicts that in the future, the double-peak structure would be resolved (the di-photon invariant mass resolution is around 1% i.e. ~ 7 GeV).

A comparison by ATLAS with the 8 TeV di-photon data and their interpretation in terms of a 750 GeV resonance implies that production by $d\bar{d}$ is disfavored at the 2.1σ level [130]. If this tendency in the data persists, we should include the contributions from strange or bottom quarks, either of which is more compatible with the 8 TeV inferred rate. Thus, instead of assuming a non-zero λ'_{i11} only, we would also be considering non-zero λ'_{ijk} where j and/or k are greater than 1. Strange or bottom quarks, being non-valence, have lower parton distribution functions to produce a 750 GeV sneutrino than down quarks and so an increase in the value of λ'_{ijk} as compared to λ'_{i11} would be required in order to fit the data.

VI. CONCLUSION AND DISCUSSION

One can explain the di-photon excess via resonant sneutrino production whilst remaining on the allowed side of other collider constraints. The model contains a stau of mass anywhere from 375 to 389 GeV and a 750 GeV sneutrino.

⁷ For a comprehensive list of LHC probes on hidden sector, see e.g. Ref. [128].

It is interesting to note that resonant left-handed slepton production has been used to simultaneously explain the ATLAS di-boson excess at 2 TeV in LHC Run I and the anomalous magnetic moment of the muon [111]. It remains to be seen whether the R -parity violating MSSM has enough freedom to simultaneously fit these measurements (which are also discrepant with SM predictions) *and* the di-photon excess addressed here. We leave the investigation of this issue to a future paper.

The most pressing concern resulting from this and other works is: will the 750 GeV $\gamma\gamma$ excess persist in future Run II data? If the answer is ‘yes’, there are some ways to discriminate our proposal from the other many new physics scenarios that have explained the excess. Firstly, the largest possible width we can get in this scenario is 0.3 GeV and so our base-line model predicts that the mild preference in the ATLAS data for a width of 45 GeV will not persist. With larger statistics, we predict that the angular distributions for the $\gamma\gamma$ final state should agree more with a spin zero resonance produced by $q\bar{q}$ initial state (as opposed to gg). Unfortunately, the γZ and ZZ signal rates are probably too small to be seen at the LHC, given that they are all suppressed by a factor of 10^4 or more compared to the $\gamma\gamma$ signal. However, the signal rates for di-jets or WW are non-negligible and while backgrounds are large, these channels remain a hope to verify the model. Charged slepton signals producing $W\gamma$ and WZ are an additional prediction of the model, at a mass very close to 750 GeV.

Note Added

In the final stages of preparation of this manuscript, Ref. [54] appeared, presenting an explanation for the di-photon excess using the sneutrino and R -parity violating supersymmetry, finding that light staus and smuons in the range 375-480 GeV are favored, and we note some overlap with our paper. However, they have not included the WW decay mode of the sneutrinos and have assumed a much larger soft SUSY-breaking term $A_{i33} = 10$ TeV, which is potentially dangerous for vacuum stability.

Acknowledgments

We thank Florian Staub and Martin Winkler for helpful communications regarding vacuum stability. The work of B.C.A. has been partially supported by STFC grant ST/L000385/1. The work of P.S.B.D. is supported in part by a TUM University Foundation Fellowship, as well as by the DFG with grant RO 2516/5-1. SR acknowledges the support of the Gordon and Betty Moore foundation during a Graduate Fellowship at the Kavli Institute for Theoretical Physics where part of this work was undertaken. This research was supported in part by the National Science Foundation under Grant No. NSF PHY11-25915.

-
- [1] Tech. Rep. ATLAS-CONF-2015-081 (2015).
 - [2] Tech. Rep. CMS-PAS-EXO-15-004 (2015).
 - [3] Tech. Rep. ATLAS-CONF-2016-018 (2016).
 - [4] Tech. Rep. CMS-PAS-EXO-16-018 (2016).
 - [5] A. Falkowski, O. Slone, and T. Volansky (2015), 1512.05777.
 - [6] K. Harigaya and Y. Nomura (2015), 1512.04850.
 - [7] Y. Mambrini, G. Arcadi, and A. Djouadi (2015), 1512.04913.
 - [8] M. Backovic, A. Mariotti, and D. Redigolo (2015), 1512.04917.
 - [9] A. Angelescu, A. Djouadi, and G. Moreau (2015), 1512.04921.
 - [10] Y. Nakai, R. Sato, and K. Tobioka (2015), 1512.04924.
 - [11] S. Knapen, T. Melia, M. Papucci, and K. Zurek (2015), 1512.04928.
 - [12] D. Buttazzo, A. Greljo, and D. Marzocca (2015), 1512.04929.
 - [13] A. Pilaftsis (2015), 1512.04931.
 - [14] R. Franceschini et al. (2015), 1512.04933.
 - [15] S. Di Chiara, L. Marzola, and M. Raidal (2015), 1512.04939.
 - [16] T. Higaki, K. S. Jeong, N. Kitajima, and F. Takahashi (2015), 1512.05295.
 - [17] J. Ellis, S. A. R. Ellis, J. Quevillon, V. Sanz, and T. You (2015), 1512.05327.
 - [18] M. Low, A. Tesi, and L.-T. Wang (2015), 1512.05328.
 - [19] B. Bellazzini, R. Franceschini, F. Sala, and J. Serra (2015), 1512.05330.
 - [20] R. S. Gupta, S. Jger, Y. Kats, G. Perez, and E. Stamou (2015), 1512.05332.
 - [21] C. Petersson and R. Torre (2015), 1512.05333.
 - [22] E. Molinaro, F. Sannino, and N. Vignaroli (2015), 1512.05334.

- [23] B. Dutta, Y. Gao, T. Ghosh, I. Gogoladze, and T. Li (2015), 1512.05439.
- [24] Q.-H. Cao, Y. Liu, K.-P. Xie, B. Yan, and D.-M. Zhang (2015), 1512.05542.
- [25] S. Matsuzaki and K. Yamawaki (2015), 1512.05564.
- [26] A. Kobakhidze, F. Wang, L. Wu, J. M. Yang, and M. Zhang (2015), 1512.05585.
- [27] R. Martinez, F. Ochoa, and C. F. Sierra (2015), 1512.05617.
- [28] P. Cox, A. D. Medina, T. S. Ray, and A. Spray (2015), 1512.05618.
- [29] D. Becirevic, E. Bertuzzo, O. Sumensari, and R. Z. Funchal (2015), 1512.05623.
- [30] J. M. No, V. Sanz, and J. Setford (2015), 1512.05700.
- [31] S. V. Demidov and D. S. Gorbunov (2015), 1512.05723.
- [32] W. Chao, R. Huo, and J.-H. Yu (2015), 1512.05738.
- [33] S. Fichet, G. von Gersdorff, and C. Royon (2015), 1512.05751.
- [34] D. Curtin and C. B. Verhaaren (2015), 1512.05753.
- [35] L. Bian, N. Chen, D. Liu, and J. Shu (2015), 1512.05759.
- [36] J. Chakraborty, A. Choudhury, P. Ghosh, S. Mondal, and T. Srivastava (2015), 1512.05767.
- [37] C. Csaki, J. Hubisz, and J. Terning (2015), 1512.05776.
- [38] A. Ahmed, B. M. Dillon, B. Grzadkowski, J. F. Gunion, and Y. Jiang (2015), 1512.05771.
- [39] P. Agrawal, J. Fan, B. Heidenreich, M. Reece, and M. Strassler (2015), 1512.05775.
- [40] D. Aloni, K. Blum, A. Dery, A. Efrati, and Y. Nir (2015), 1512.05778.
- [41] Y. Bai, J. Berger, and R. Lu (2015), 1512.05779.
- [42] E. Gabrielli, K. Kannike, B. Mele, M. Raidal, C. Spethmann, and H. Veerme (2015), 1512.05961.
- [43] R. Benbrik, C.-H. Chen, and T. Nomura (2015), 1512.06028.
- [44] J. S. Kim, J. Reuter, K. Rolbiecki, and R. R. de Austri (2015), 1512.06083.
- [45] A. Alves, A. G. Dias, and K. Sinha (2015), 1512.06091.
- [46] E. Megias, O. Pujolas, and M. Quiros (2015), 1512.06106.
- [47] L. M. Carpenter, R. Colburn, and J. Goodman (2015), 1512.06107.
- [48] J. Bernon and C. Smith (2015), 1512.06113.
- [49] W. Chao (2015), 1512.06297.
- [50] M. T. Arun and P. Saha (2015), 1512.06335.
- [51] C. Han, H. M. Lee, M. Park, and V. Sanz (2015), 1512.06376.
- [52] S. Chang (2015), 1512.06426.
- [53] I. Chakraborty and A. Kundu (2015), 1512.06508.
- [54] R. Ding, L. Huang, T. Li, and B. Zhu (2015), 1512.06560.
- [55] H. Han, S. Wang, and S. Zheng (2015), 1512.06562.
- [56] X.-F. Han and L. Wang (2015), 1512.06587.
- [57] M.-x. Luo, K. Wang, T. Xu, L. Zhang, and G. Zhu (2015), 1512.06670.
- [58] J. Chang, K. Cheung, and C.-T. Lu (2015), 1512.06671.
- [59] D. Bardhan, D. Bhatia, A. Chakraborty, U. Maitra, S. Raychaudhuri, and T. Samui (2015), 1512.06674.
- [60] T.-F. Feng, X.-Q. Li, H.-B. Zhang, and S.-M. Zhao (2015), 1512.06696.
- [61] O. Antipin, M. Mojaza, and F. Sannino (2015), 1512.06708.
- [62] F. Wang, L. Wu, J. M. Yang, and M. Zhang (2015), 1512.06715.
- [63] J. Cao, C. Han, L. Shang, W. Su, J. M. Yang, and Y. Zhang (2015), 1512.06728.
- [64] F. P. Huang, C. S. Li, Z. L. Liu, and Y. Wang (2015), 1512.06732.
- [65] W. Liao and H.-q. Zheng (2015), 1512.06741.
- [66] J. J. Heckman (2015), 1512.06773.
- [67] M. Dhuria and G. Goswami (2015), 1512.06782.
- [68] X.-J. Bi, Q.-F. Xiang, P.-F. Yin, and Z.-H. Yu (2015), 1512.06787.
- [69] J. S. Kim, K. Rolbiecki, and R. R. de Austri (2015), 1512.06797.
- [70] L. Berthier, J. M. Cline, W. Shepherd, and M. Trott (2015), 1512.06799.
- [71] W. S. Cho, D. Kim, K. Kong, S. H. Lim, K. T. Matchev, J.-C. Park, and M. Park (2015), 1512.06824.
- [72] J. M. Cline and Z. Liu (2015), 1512.06827.
- [73] M. Bauer and M. Neubert (2015), 1512.06828.
- [74] M. Chala, M. Duerr, F. Kahlhoefer, and K. Schmidt-Hoberg (2015), 1512.06833.
- [75] D. Barducci, A. Goudelis, S. Kulkarni, and D. Sengupta (2015), 1512.06842.
- [76] S. M. Boucenna, S. Morisi, and A. Vicente (2015), 1512.06878.
- [77] C. W. Murphy (2015), 1512.06976.
- [78] A. E. C. Hernandez and I. Nisandzic (2015), 1512.07165.
- [79] U. K. Dey, S. Mohanty, and G. Tomar (2015), 1512.07212.
- [80] G. M. Pelaggi, A. Strumia, and E. Vigiani (2015), 1512.07225.
- [81] J. de Blas, J. Santiago, and R. Vega-Morales (2015), 1512.07229.
- [82] P. S. B. Dev and D. Teresi (2015), 1512.07243.
- [83] W.-C. Huang, Y.-L. S. Tsai, and T.-C. Yuan (2015), 1512.07268.
- [84] S. Moretti and K. Yagyu (2015), 1512.07462.
- [85] K. M. Patel and P. Sharma (2015), 1512.07468.
- [86] M. Badziak (2015), 1512.07497.

- [87] S. Chakraborty, A. Chakraborty, and S. Raychaudhuri (2015), 1512.07527.
- [88] Q.-H. Cao, S.-L. Chen, and P.-H. Gu (2015), 1512.07541.
- [89] W. Altmannshofer, J. Galloway, S. Gori, A. L. Kagan, A. Martin, and J. Zupan (2015), 1512.07616.
- [90] M. Cvetič, J. Halverson, and P. Langacker (2015), 1512.07622.
- [91] J. Gu and Z. Liu (2015), 1512.07624.
- [92] U. Ellwanger and C. Hugonie (2016), 1602.03344.
- [93] F. Domingo, S. Heinemeyer, J. S. Kim, and K. Rolbiecki (2016), 1602.07691.
- [94] M. Badziak, M. Olechowski, S. Pokorski, and K. Sakurai (2016), 1603.02203.
- [95] J. A. Casas, J. R. Espinosa, and J. M. Moreno (2015), 1512.07895.
- [96] R. Ding, Y. Fan, L. Huang, C. Li, T. Li, S. Raza, and B. Zhu (2016), 1602.00977.
- [97] D. Bardhan, P. Byakti, D. Ghosh, and T. Sharma (2016), 1603.05251.
- [98] Tech. Rep. CMS-PAS-EXO-14-005 (2015).
- [99] G. Aad et al. (ATLAS), Phys. Rev. **D91**, 052007 (2015), 1407.1376.
- [100] G. Passarino and M. J. G. Veltman, Nucl. Phys. **B160**, 151 (1979).
- [101] A. Denner, Fortsch. Phys. **41**, 307 (1993), 0709.1075.
- [102] T. Hahn and M. Perez-Victoria, Comput. Phys. Commun. **118**, 153 (1999), hep-ph/9807565.
- [103] V. Khachatryan et al. (CMS), JHEP **10**, 144 (2015), 1504.00936.
- [104] G. Aad et al. (ATLAS), JHEP **01**, 032 (2016), 1509.00389.
- [105] A. Alloul, N. D. Christensen, C. Degrande, C. Duhr, and B. Fuks, Comput. Phys. Commun. **185**, 2250 (2014), 1310.1921.
- [106] J. Alwall, R. Frederix, S. Frixione, V. Hirschi, F. Maltoni, O. Mattelaer, H. S. Shao, T. Stelzer, P. Torrielli, and M. Zaro, JHEP **07**, 079 (2014), 1405.0301.
- [107] R. D. Ball et al., Nucl. Phys. **B867**, 244 (2013), 1207.1303.
- [108] V. Khachatryan et al. (CMS) (2016), 1604.08907.
- [109] G. Aad et al. (ATLAS) (2015), 1512.01530.
- [110] V. Khachatryan et al. (CMS) (2015), 1512.01224.
- [111] B. C. Allanach, P. S. B. Dev, and K. Sakurai (2015), 1511.01483.
- [112] A. Salvio, F. Staub, A. Strumia, and A. Urbano (2016), 1602.01460.
- [113] R. Barbier et al., Phys. Rept. **420**, 1 (2005), hep-ph/0406039.
- [114] F. Goertz, J. F. Kamenik, A. Katz, and M. Nardecchia (2015), 1512.08500.
- [115] F. Staub et al. (2016), 1602.05581.
- [116] M. Herz, Ph.D. thesis, Bonn U. (2002), hep-ph/0301079.
- [117] H. K. Dreiner, M. Kramer, and B. O’Leary, Phys. Rev. **D75**, 114016 (2007), hep-ph/0612278.
- [118] A. de Gouvea, S. Lola, and K. Tobe, Phys. Rev. **D63**, 035004 (2001), hep-ph/0008085.
- [119] J. Adam et al. (MEG), Phys. Rev. Lett. **110**, 201801 (2013), 1303.0754.
- [120] M. Frank and H. Hamidian, J. Phys. **G24**, 2203 (1998), hep-ph/9706510.
- [121] J. Baron et al. (ACME), Science **343**, 269 (2014), 1310.7534.
- [122] R. N. Mohapatra, Phys. Rev. **D34**, 3457 (1986).
- [123] M. Hirsch, H. V. Klapdor-Kleingrothaus, and S. G. Kovalenko, Phys. Rev. **D53**, 1329 (1996), hep-ph/9502385.
- [124] M. Agostini et al. (GERDA), Phys. Rev. Lett. **111**, 122503 (2013), 1307.4720.
- [125] A. Faessler, S. Kovalenko, F. Simkovic, and J. Schwieger, Phys. Rev. Lett. **78**, 183 (1997), hep-ph/9612357.
- [126] B. C. Allanach, C. H. Kom, and H. Pas, JHEP **10**, 026 (2009), 0903.0347.
- [127] G.-C. Cho and K. Hagiwara, Nucl. Phys. **B574**, 623 (2000), hep-ph/9912260.
- [128] J. Jaeckel, M. Jankowiak, and M. Spannowsky, Phys. Dark Univ. **2**, 111 (2013), 1212.3620.
- [129] V. Khachatryan et al. (CMS), JHEP **11**, 071 (2015), 1506.08329.
- [130] M. Delmastro, in *Rencontres de Moriond Electroweak Session* (2016).